The Journal of Experimental Biology 213, 1241-1250

doi:10.1242/jeb.038661

It's tough to be small: dependence of burrowing kinematics on body size

James Che and Kelly M. Dorgan*

University of California, Berkeley, Department of Integrative Biology, 3060 VLSB #3140, Berkeley, CA 94720, USA

*Author for correspondence (kelly.dorgan@berkeley.edu)

Accepted 7 January 2010

SUMMARY

Burrowing marine infauna are morphologically diverse and range in size over several orders of magnitude. Whilst effects of ontogenetic and morphological differences on running, flying and swimming are relatively well understood, similar analyses of burrowing mechanics and kinematics are lacking. The polychaete *Nereis virens* Sars extends its burrow by fracture, using an eversible pharynx to exert force on the walls of the burrow. The resulting stress is amplified at the anterior tip of the burrow, which extends when the stress exceeds the fracture toughness of the material. Here we show that the polychaete *Cirriformia moorei* extends its burrow by a similar mechanism, but by using its hydrostatic skeleton rather than an eversible pharynx. Based on the dimensionless wedge number, which relates work of fracture to work to maintain body shape against the elasticity of sediment, we predicted that smaller worms would exhibit behaviors characteristic of tougher sediments and that scaling of kinematics would reflect decreasing difficulty in fracturing sediment with increasing body size. We found that smaller worms were relatively blunter and thicker, and had a greater variation of thickness than larger worms as they burrowed. Although these kinematic differences increase the stress amplification at the crack tip, smaller worms still generate lower stress intensity factors. The greater relative body thickness and shape changes of smaller worms are consistent with ontogenetic changes in forces exerted by earthworms, and are likely driven by the challenge of exerting enough stress to extend a crack with a small body size.

Supplementary material available online at http://jeb.biologists.org/cgi/content/full/213/8/1241/DC1

Key words: sediment mechanics, burrowing mechanics, biomechanics, Cirratulidae, *Cirriformia moorei*, gelatin, fracture, locomotion, peristalsis, ontogenetic scaling, hydrostatic skeleton.

INTRODUCTION

Muddy marine sediments are elastic solids through which burrowers move by extending crack-shaped burrows (Dorgan et al., 2005). Through burrowing and feeding activities, marine infauna alter the structure of the sediment, affecting the fate of organic carbon and nutrients to such an extent that they are considered ecosystem engineers (Meysman et al., 2006). Recently, we have shown that kinematics and behaviors of burrowers depend on the mechanical properties of the medium through which they burrow (Dorgan et al., 2008). Burrowing kinematics, however, have only been described for one species, *Nereis virens* Sars; here, we examine the ubiquity of crack propagation by describing kinematics and mechanics of burrowing by an anatomically different worm, *Cirriformia moorei* (Blake, 1996). We also extend our research on how burrowing behavior depends on sediment properties by examining how that interaction depends on body size.

Burrowing by crack propagation

Nereis virens burrows by crack propagation, as observed with video analysis of burrowing in gelatin, which acts as a mechanical analog for muddy sediments (Dorgan et al., 2005; Dorgan et al., 2007). An oblate spheroidal (tongue-depressor shaped) crack compresses the worm dorsoventrally and extends laterally away from the worm. The worm uses its body wall musculature and hydrostatic skeleton to develop coelomic pressure and maintain its body shape in the elastic medium. *Nereis virens* burrows by everting its pharynx, exerting dorsoventral forces against the crack walls, and driving the pharynx forward in the crack as it everts (Dorgan et al., 2007). Pharynx eversion is not necessary to extend the crack, however, and worms exhibit different burrowing behaviors, varying body thickness and the occurrence and extent of side-to-side head movements and pharynx eversions, in media with different mechanical properties (Dorgan et al., 2008). In all cases, the worm acts as a wedge, and the force exerted near the crack tip is amplified at the tip to cause the crack to extend anteriorly away from the worm (Dorgan et al., 2008).

We have suggested that the mechanism of burrowing by crack propagation is widespread in muddy sediments (Dorgan et al., 2006), and here we examine the kinematics of burrowing by the cirratulid polychaete *C. moorei*, and compare the mechanics of burrowing with those of *N. virens*. Whereas *N. virens* everts its pharynx to exert a dorsoventral force on the crack walls and moves forward with a combination of undulation and peristalsis, *C. moorei* does not use pharynx eversion and has a less rigid body wall, enabling greater changes in shape using its hydrostatic skeleton. Preliminary observations using photoelastic stress analysis (see Dorgan et al., 2007) of *C. moorei* burrowing in gelatin suggest that forces are less focused and that stress is applied along a greater length of the body. We hypothesize that *C. moorei* uses its hydrostatic skeleton to change its body shape to burrow by crack propagation in a manner analogous to pharynx eversion by *N. virens*. In addition to using different anatomical features from *N. virens* to burrow, cirratulid burrowing is likely similar to that of other less rigid-bodied polychaete burrowers (e.g. Cossuridae). Additionally, the Cirratulidae are abundant in intertidal mudflats, as well as subtidally to great depths, and are important bioturbators of muddy sediments (see Shull and Yasuda, 2001). They are typically the most abundant species in deep-sea communities (Jumars and Gallagher, 1982).

Ontogenetic effects on burrowing

Marine infaunal animals settle into muddy sediments as microscopic larvae and can grow up to several orders of magnitude in size, over which their perception of their physical environment changes from a boulder field of sediment grains that are very large relative to body size to a continuum of small particles suspended in a mucopolymeric matrix of organic material. This change in the relative size of sediment grains to body size has been shown to be important for animals feeding on sediment grains; ontogenetic changes in deposit feeding have been observed in polychaetes (Hentschel, 1998; Mahon and Dauer, 2005) and clams (Rossi et al., 2004). Because limited gut volume accompanies small body size, juvenile deposit feeders select for small, high-nutrient food particles (Penry and Jumars, 1990), including higher nutrient microalgae (Hentschel, 1998; Rossi et al., 2004). The ratios of body and gut sizes to sediment grain size are important in feeding because organic content scales with the surface area rather than the volume of mineral grains (Mayer et al., 1993). The relative size of sediment grains is likely important for the mechanics of burrowing as well, but this question has not been explicitly addressed. Muddy sediments are elastic gels whose mechanics are governed by the adhesive (organic material sticking to grains) and cohesive (organic material sticking to itself) forces in the mucopolymeric matrix of organic material in which sediment grains are held (Dorgan et al., 2006). To small burrowers whose sizes do not greatly exceed the size of sediment grains, the behavior of individual grains becomes more important, and the assumptions of continuum mechanics are no longer appropriate (Johnson et al., 2002; Boudreau et al., 2005; Dorgan et al., 2006). In other words, the mechanical response of sediments to forces on spatial scales much larger than that of individual grains is to deform elastically, storing elastic energy that can be released by fracture (see Johnson et al., 2002). Even for worms large enough that the sediment behaves like a continuum, the effect of body size on burrowing mechanics is not well understood. Here we take the first step in understanding ontogenetic changes in burrowing by comparing burrowing mechanics within the size range for which sediment behaves like a continuum.

Ontogenetic changes in crawling by terrestrial earthworms large enough that soil behaves like a continuum have been documented. Earthworms maintain geometric similarity as well as static and dynamic stress (forces per cross-sectional area within a still and moving body wall, respectively) similarity over large size ranges (Quillin, 1998). Crawling by earthworms in artificially made tunnels also shows kinematic similarity (Quillin, 1999). Both radial and axial forces exerted by earthworms, however, scale with mass to the power of 2/5 rather than 2/3 as predicted by geometric similarity, so larger worms exert smaller forces relative to their body size than predicted by similarity (Quillin, 2000). The mechanics of burrowing and crawling differ, however, as burrowers in muddy sediments exert forces against the walls of a crack to extend the burrow by fracture, whereas crawlers do work against friction to move forward along a surface (K.M.D., unpublished observations).

Predictions from fracture mechanics

The external work for a worm to burrow is composed of two key components: the work to fracture the crack a distance Δx, W_{Cr} (Eqn 1), and the work to deform the elastic material to allow space for the worm's body, W_{El} (Eqn 2). The work of fracture depends on the fracture toughness of the material, G_c (J m^{-2}), which is the energy required to create new crack surface area, and the total new surface area formed, or the product of the crack width, w_{crack}, and distance of crack growth, Δx (Dorgan et al., 2008):

$$W_{Cr} = G_c w_{crack} \Delta x \, . \quad (1)$$

The work to deform the elastic material depends on the stiffness or elastic modulus, E (Pa), as well as how far the material is deformed, here the half-thickness of the worm. Worm thickness varies along the length of the worm as well as over time, but we consider half-thickness, h, in the middle region of the worm (far from the crack tip) at the time the crack is extending anteriorly (Dorgan et al., 2008):

$$W_{El} \propto E h w_{worm} \Delta x \, . \quad (2)$$

Here, the components of elastic work and work of fracture depend on the widths of the worm w_{worm} (m) and the crack w_{crack} (m), respectively.

The dependence of burrowing behavior on the mechanical properties of sediments has been characterized using the dimensionless 'wedge' number, Wg, which represents the ratio of the work to extend the burrow by fracture (W_{Cr}) to the work against the sediment's elastic restoring force (W_{El}) (Dorgan et al., 2008):

$$\mathrm{Wg} = \frac{W_{Cr}}{W_{El}} = \frac{G_c}{Eh} \times \frac{w_{crack}}{w_{worm}} \, . \quad (3)$$

The wedge number depends not only on the mechanical properties of sediments but also on the thickness, h, of the worm while burrowing and therefore can be used to predict differences in burrowing behavior among worms of varying body sizes. As the toughness of the material increases, worms must increase their thickness h to apply enough stress to exceed the fracture toughness and propagate the crack. Smaller worms have smaller thicknesses and therefore have more difficulty exerting enough stress to fracture the sediment, which appears tougher than for larger worms. In other words, fracturing the sediment is an issue for small worms for which the wedge number is high, and maintaining body shape against the elasticity of the sediment is an issue for larger worms at lower wedge numbers.

When *N. virens* extends its burrow by fracture, the tip of the crack extends as the worm drives the everting pharynx into the crack like a wedge (Dorgan et al., 2007). Burrow extension has been modeled as 2D wedge-driven fracture using an analytical solution for the stress intensity factor (K_I) of a stable crack formed from an arbitrary 2D wedge profile (Dorgan et al., 2008). The stress intensity factor, K_I (Pa m$^{0.5}$), describes the amplification of stress at the crack tip from a load applied perpendicular to the walls of a crack (termed 'mode I loading'). When enough stress is applied, K_I exceeds the critical stress intensity factor, K_{Ic}, referred to as the fracture toughness of the material, and the crack extends (Anderson, 1995). The fracture toughness, K_{Ic} [Pa m$^{0.5}$], is a measure of the amount of stress at the crack tip during fracture, and is related to the energy-based fracture toughness, G_c, through the elastic modulus, E (Pa), and Poisson's ratio, ν (dimensionless) (the ratio of transverse strain to axial strain under an applied load on the material), which are all material properties of elastic solids (Anderson, 1995):

$$G_c = \frac{K_{Ic}^2 \left(1 - \nu^2\right)}{E} \, . \quad (4)$$

When the tip of a crack is extended at a slow and steady rate using a wedge of arbitrary shape, the stress intensity factor can be calculated as (Sih, 1973):

$$K_I = \frac{E\sqrt{2a}}{2\sqrt{\pi}\,(1-\nu)^2} \int_a^\infty \frac{f'(z-b)}{\sqrt{z(z-a)}}\,\mathrm{d}z, \;\; a > b \, . \quad (5)$$

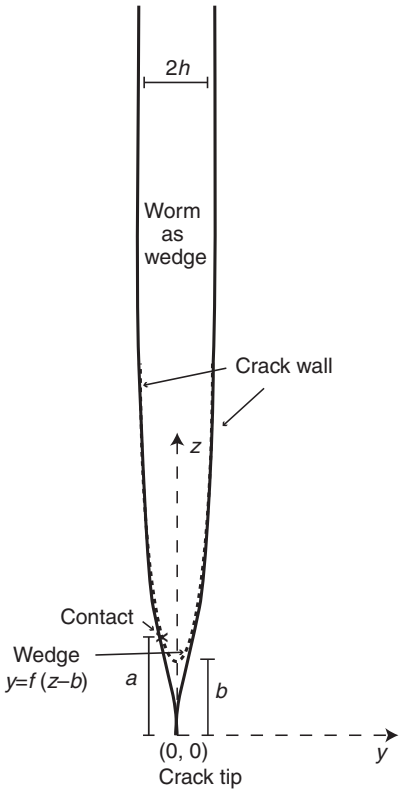

Fig. 1. A worm as a wedge (dotted line) with an arbitrary profile $y=\pm f(z–b)$ extending a crack (solid line) in a solid. The distances *b*, between the tip of the crack and the anterior end of the wedge, and *a*, between the tip of the crack and the point of contact between the worm and the crack wall, and half-thickness *h*, far from the anterior of the worm, are indicated (modified from Dorgan et al., 2008).

As shown in Fig. 1, b is the distance from the tip of the wedge (the anterior end of the worm) to the crack tip. The crack tip is assumed to be at the maximum distance that the anterior of the worm has reached. The function $f(z–b)$ is the shape of the wedge, here the half-thickness along the length of the worm (along the z-axis), which can be measured from the lateral view video of worms burrowing in gelatin, a clear analog for muddy sediments (see Materials and methods). Eqn 5 depends on $f'(z–b)$, the slope of the worm profile, and worms with higher slopes at the anterior end are blunter than other worms as they burrow. The distance, a, between the crack tip and the point of contact of the worm's body with the crack wall is difficult to measure, as the anterior end of the worm is very close to the burrow wall but does not actually exert stress that contributes to K_I. Because we had one equation with two unknowns, we needed another equation to solve for both K_I and a. We used another equation for K_I that includes a as well as h, the half-thickness (m) of the wedge at infinity (here the half-thickness of the worm's body far from the anterior end), and solved the two equations simultaneously [following previously published methods (Dorgan et al., 2008)] (Barenblatt, 1962):

$$K_I = \frac{E}{\sqrt{2\pi a}(1-\nu^2)}\left(h - \int_a^\infty f'(z-b)\sqrt{\frac{z-a}{z}}\,dz\right). \quad (6)$$

From the wedge equation (Eqn 3), we hypothesize that smaller worms (with smaller h) should differ in burrowing behavior from larger worms in ways that increase K_I. Specifically, we expect body size to have a negative correlation with relative body thickness (the $f(z–b)$ term), changes in relative body thickness (amplitude of peristaltic wave), and maximum slope (bluntness) at the point of contact, m_a, during burrowing. We also hypothesize that these changes in behavior of small worms would be insufficient to raise the stress intensity to the level that large worms can achieve; in other words, stress intensity factor will show a positive correlation with body size. In summary, we predict that smaller worms are relatively thicker and blunter while burrowing in order to increase the stress intensity factor and extend their burrow by fracture.

MATERIALS AND METHODS

Animals

A range of sizes (0.01–0.44 g) of the cirratulid polychaete *C. moorei* were collected to analyze burrowing kinematics and behavior with respect to body size. Animals were taken from Doran Regional Park, Bodega Bay, CA, USA, and Inverness, Tomales Bay, CA, USA, at low tide and kept at 11°C in containers of mud and aerated seawater until use.

Gelatin as an analog for muddy sediments

Study of the locomotion of subterranean organisms has been impeded by the inability to visualize movement through the substrata and a lack of understanding of burrowing mechanics. Gelatin in seawater has been used as an analog for muddy sediments based on similar mechanical properties (Johnson et al., 2002; Dorgan et al., 2005; Boudreau et al., 2005). Bubbles in both media grow by fracture, and the shape of the bubble depends on the ratio of the fracture toughness, K_{Ic}, to the stiffness, E, of the medium. Bubbles in gelatin and muddy sediments have similar aspect ratios, the ratio of the half-thickness (δ_c) to half-width (a_c) of the bubble once it stops growing (Johnson et al., 2002).

Both K_{Ic} and E are larger for muddy sediment than for gelatin. However, the K_{Ic}/E ratios – which are directly proportional to the aspect ratios – of the two media coincide. Gelatin thus exhibits similar cracking behavior to mud.

Gelatin has been used as an analog for mud in experiments to analyze the behavior of worms and the mechanism of burrowing by crack propagation (Dorgan et al., 2005; Dorgan et al., 2007; Dorgan et al., 2008). Sediment stores elastic energy much less effectively than gelatin [see figure 4 in Dorgan et al. (Dorgan et al., 2007)], and this difference may be important in long-term behavioral studies. Over the short periods in this study, however, gelatin is an effective transparent medium for observing burrowing mechanics in *C. moorei*.

Experimental setup

The experimental setup was similar to that described previously (Dorgan et al., 2007; Dorgan et al., 2008). A clear glass container of gelatin was positioned in between a Porta-Trace (Gagne, Inc., Johnson City, NY, USA) light table and a CCD video camera (Basler A622f, Exton, PA, USA) with circular polarizers. Experiments were done in a cold room at 11°C. Gelatin (www.bulkfoods.com) was boiled at high concentration in an artificial seawater solution (Instant Ocean, Aquarium Systems, Inc., Mentor, OH, USA). Afterwards, additional artificial seawater was added to dilute the solution and obtain the selected concentration (28.35 g l^{-1} seawater), and the containers of gelatin were cooled overnight before use.

Video footage

Video footage of burrowing was acquired for both the lateral and dorsal view of *C. moorei*. For dorsal view video recordings, the tank was positioned such that the camera's line of sight was normal

to the plane of the crack. The lateral view is such that the plane of the crack is parallel to the direction of the camera. Branchial filaments and the width of the worm's body were visible in the dorsal view. Filaments, however, were masked in lateral view by the worm's body (Fig. 2).

In preparation for video footage, forceps were used to make a small crack in the gelatin. The worm was placed in the crack, and recording was initiated once it began to burrow downward. Video was acquired using LabView software (version 7.1.1, National Instruments, Austin, TX, USA) at 3.75 frames s^{-1}. The lens on the video camera had a fixed focal length, and the camera was moved to keep the worm in focus while it burrowed. Constant distance between the worm and the camera allowed accurate measurements of body thicknesses and widths. Polarizers were oriented to obtain satisfactory outlines of the burrowing worms so that the dark shape of the worm in each frame could be distinguished on a light background. The position of the camera remained fixed until the worm traveled out of the camera's field of view. Worms for which video footage was not immediately rejected were preserved in formalin. Mass, length, width at the fourth and eighth setigers, and thickness at the fourth and eighth setigers of preserved worms were later measured.

Several factors were considered in determining whether videos were included in analysis. Only segments of videos in which the worm moved at least four burrowing cycles without stopping, changing direction or moving out of the field of view were used. Videos in which the angle of the worm from the vertical axis towards or away from the camera exceeded 20 deg. were rejected, as this could result in inaccurate measurements of thickness or width. Also, in order to limit the effects of the tank wall on gelatin, only video segments of worms burrowing more than 0.015 m from the wall were used. Each worm was only used once, and data presented are the averages of at least four burrowing cycles.

For lateral view videos, the worms must be burrowing within a plane parallel to the camera view. Videos with shading and dark regions (caused by uneven light distributions) were excluded since these patches interfered with lateral image analysis to obtain contours of the worm body shape. In addition, videos in which worms were twisted, identified by visibility of the gills in the lateral view of the worm, were rejected from the analysis. Emphasis was placed on acquiring lateral view videos, since worm thickness is an important parameter in the wedge model. For dorsal view videos, the worms must be burrowing within a plane perpendicular to the camera view.

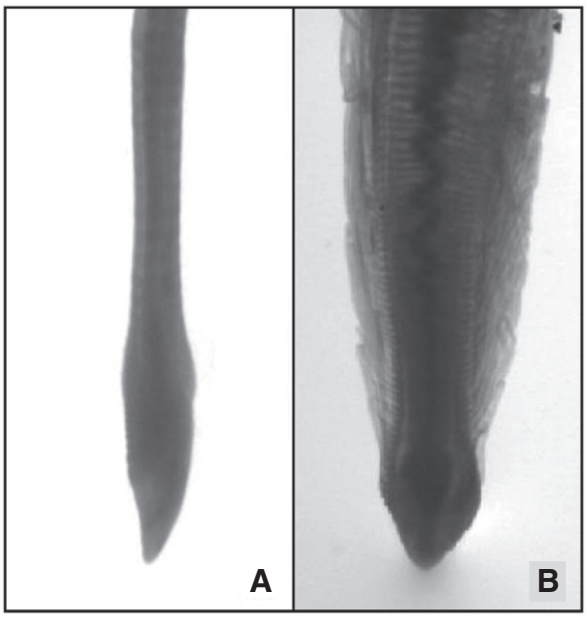

Fig. 2. Lateral (A) and dorsal (B) images *of Cirriformia moorei* in gelatin. The gills are masked in the lateral view by the thickness of the worm but are clearly visible in the dorsal view extending laterally in the crack.

Lateral view data analysis

Video segments fitting the above criteria were sub-sampled using LabView. Lateral view video was used since the dorsal and ventral sides of the worm exert force against the crack walls, and the resulting deformation (body thickness of the worm) is used in the wedge model to calculate the stress intensity factor.

The thickness of the worm along the central body axis [specifying the function $f(z–b)$ in Eqns 5 and 6], was measured at each frame. Contours around the worm's body in lateral view videos were obtained using ProAnalyst (Xcitex, Inc., Cambridge, MA USA), and x and y coordinates of each point on the contour (>200 points per contour) were exported as Excel (Microsoft, Redmond, WA, USA) documents. From the contour points, Matlab (R2007a; The Mathworks, Inc., Natick, MA, USA) was used to calculate body thickness along the length axis of the worm [to arrive at the function $f(z–b)$ in Eqns 5 and 6]. Because the two sides of the worm curved slightly, we had to match the appropriate points along the contour line to obtain a thickness. First, a linear regression was made through roughly calculated midpoints along the body contour, generating a midline passing through the central body axis. At each point (p_r) along this regression line, Matlab was used to find the two points along the contour of the worm (one for each side of the worm) where the slope between each point and p_r is perpendicular to the slope at p_r. The distance between the two points is the thickness of the worm at the midpoint p_r. For a worm burrowing straight down with evenly spaced contour points, this procedure is equivalent to taking the horizontal thickness of the contour at each midpoint.

From the body thicknesses, the stress intensity factor (K_I), distance from the crack tip to the point of contact between the worm body and crack wall (a), and slope of the body wall at the point of contact (m_a) were calculated. Note that the point of contact changes over a burrowing cycle, ranging from a minimum distance from the anterior of the worm, a_{min}, to a maximum, a_{max}. Distance traveled between each time frame was calculated from the difference in position of the anterior tip of the worm; overall speed, period of each stride, and distance between the anterior of the worm and the crack tip (b) were calculated from distance traveled. In addition, variability in thicknesses and lags between time-dependent variables (K_I, a, m_a and thickness along the worm body), were also calculated for each worm.

The crack was assumed to extend only as far as the anterior tip of the worm (see Dorgan et al., 2007; Dorgan et al., 2008), and the distance from the anterior end of the worm to the tip of the crack (b) was calculated from the maximum distance the worm traveled. This assumption is valid if the calculated stress intensity factors (K_I) do not greatly exceed the critical stress intensity factor (in which case the crack extends beyond the tip of the worm) (Dorgan et al., 2008). The value a could not be found by direct inspection of video data. As such, values for a and K_I were calculated by iteratively increasing a until K_I values, given by Eqns 5 and 6, were within a tolerance of 2 Pa $m^{0.5}$. The two K_I values were averaged as the solution. A unique solution to the two equations is guaranteed by elasticity theory (Timoshenko and Goodier, 1970).

Fluctuations in thickness at several points were analyzed over time. The thickness of the anterior of the worm is important because stress near the crack tip has a greater contribution to the stress

intensity factor (see Eqn 5), so thickness was measured at a_{min}, a_{max}, and a distance 1/20th of the worm length away from the anterior end. The thickness h was also measured.

Time lags were calculated by finding the local maxima of the two variables of interest and averaging the time differences between the peaks of the two variables. The variables included stress intensity factor (K_I), distance traveled, slope at the point of contact (m_a) and thickness at the anterior point of contact (a_{min}).

The position of the tip of the head was determined as the point closest to the bottom of the field of view for worms burrowing downward in the aquarium at each time frame. Total distance traveled was calculated as the distance between the position of the head tip in a given frame and that of the initial frame. Linear distance is appropriate because worms burrowed in a fairly straight line.

Speed was calculated from a plot of the total distance traveled as a function of time. Over a burrowing cycle, worms move forward but then back up a fraction of the forward distance. The slope of the best-fit line through the local maxima of the distances is the average speed of the worm. Distance traveled per stride was calculated as the average difference between sequential local maxima. The period of a stride was calculated by averaging the time differences between these local maxima.

Dorsal view video analysis

From dorsal view videos, widths of worms were measured every 5 frames over three burrowing cycles using LabView. For each frame, the location of the anterior end was recorded, and 10 width measurements were made along the body. Matlab was used to interpolate through the 10 width measurements to obtain the body shape of the worm. Distance and speed of travel were obtained from these data using the same methods as applied in lateral view videos.

Normalized burrowing widths were calculated to compare body shapes among worms of different body sizes. Widths were measured at several distances from the anterior end, normalized by dividing by the measured width of preserved worms at the eighth setiger, and compared among body sizes using Matlab.

Analysis of size effects

The software Mystat (Systat Software, Inc., Chicago, IL, USA) was used to calculate R^2 and P values for the regressions. One-sided t-tests were used to determine the significance of correlations. Because specific hypotheses were generated for each variable based on theory, statistical significance of each test was calculated independently of other tests.

Variables that are dependent on body size were normalized to the width of the specific worm by dividing by its width at the eighth setiger. These variables include thickness in gelatin, changes in thickness, and values of a_{min} and a_{max}. Subsequent results refer to relative measurements – rather than absolute measurements – in which normalization was applied for the appropriate variables.

RESULTS

Animals

The 21 worms used to acquire lateral view videos and the seven worms used for dorsal view videos ranged in preserved length from 1.6 to 4.0 cm, wet mass from 0.01 to 0.50 g, width of the eighth setiger from 1.06 to 2.94 mm, and thickness at the eighth setiger from 0.91 to 2.63 mm. Width (in mm) and mass (in g) are strongly correlated, as expected, with a slightly stronger correlation using the cubed root of mass: R^2=0.88 and mass$^{1/3}$=3.02×width+0.43. Since some worms may have been regenerating broken tails, the width at the eighth setiger, rather than mass, was used as an indication of body size.

Burrowing kinematics

Discrete burrowing cycles can be distinguished from a plot of distance traveled as a function of time (Fig. 3A). During each burrowing cycle, the position of the anterior end of the worm extends forward to reach the previous maximum distance, moves forward and extends the burrow, reaches a new maximum distance traveled, and then moves back. We have defined these four stages as forward stretching, anterior crack extension, anterior body thickening and peristaltic wave progression, respectively.

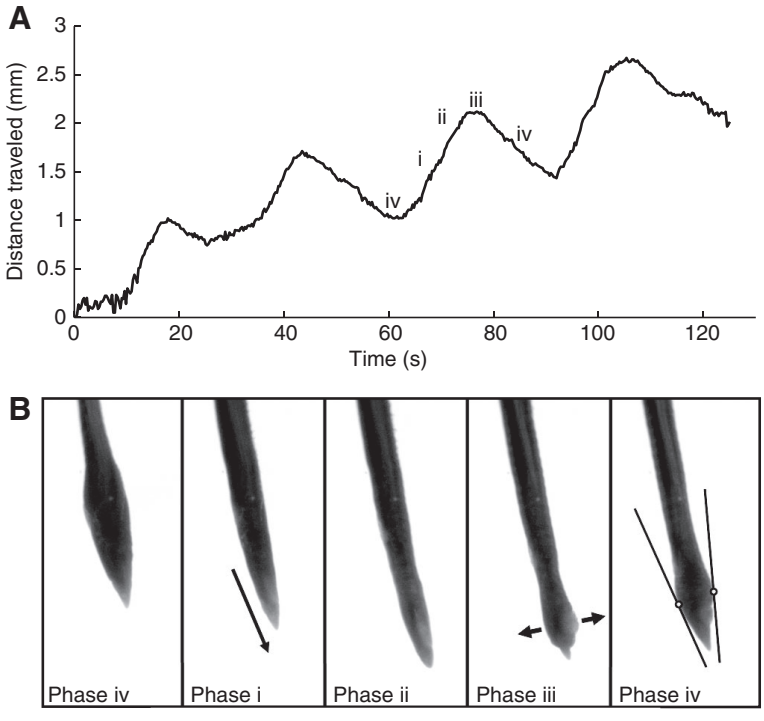

Fig. 3. (A) Distance traveled over time for a representative worm (0.32 g wet mass). (B) Time-lapse lateral view images of *C. moorei* showing four phases of burrowing: forward stretching (phase i), anterior crack extension (phase ii), anterior body thickening (phase iii) and peristaltic wave progression (phase iv). The slope at the point of contact (shown in the last image) peaks in phase iii then decreases in phase iv and subsequent phases.

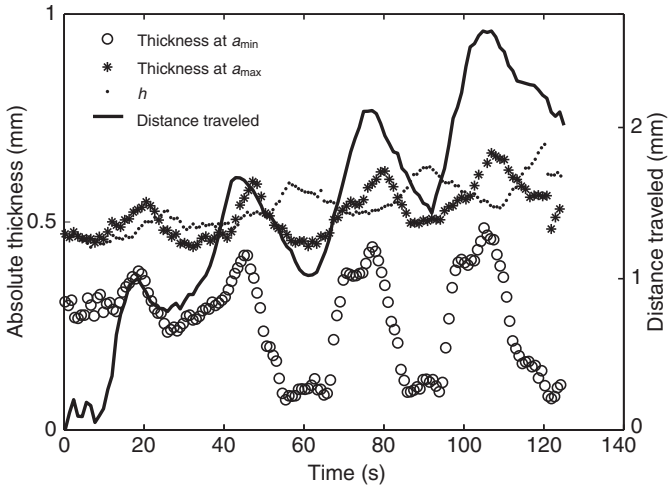

Fig. 4. Thickness at the minimum (open circles) and maximum (asterisks) points of contact (a_{min} and a_{max}, respectively) and the thickness h (solid circles) far from the anterior of the worm over several burrowing cycles. Also shown is the distance traveled (solid line) to indicate when the changes in thickness occur.

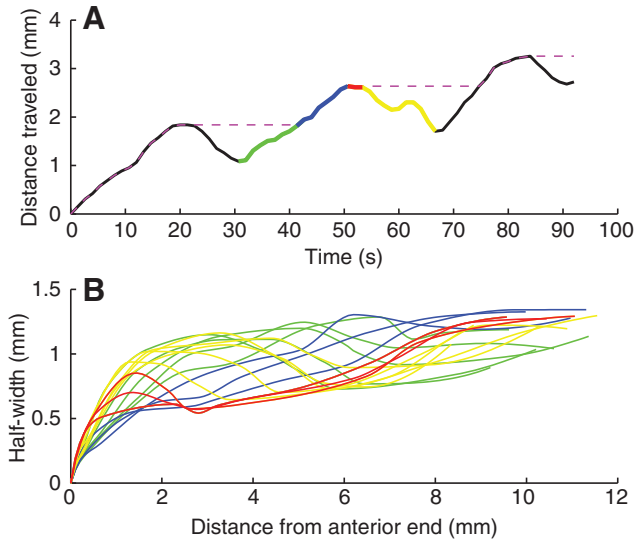

Fig. 6. (A) Distance traveled over time for a representative worm (0.32 g wet mass). The location of the crack tip, assumed to be at the farthest point traveled by the worm (dashed magenta line), is shown. (B) Half-widths of the worm body at different times in the burrowing cycle. Body shape during forward stretching (green), anterior crack extension (blue), anterior body thickening (red) and peristaltic wave progression (yellow) are indicated.

The shape of the worm changes over the burrowing cycle as well (Fig. 3B). The thickness h and the thickness at a_{min} and a_{max} each exhibited regular, consistent fluctuations (Fig. 4). Note that changes in thickness at a_{min} near the crack tip greatly affect the stress intensity factor. There were three distinct levels of thickness at a_{min}. Thickness was at a minimum as the worm began moving forward (increase in distance traveled). An intermediate level was reached as distance surpassed the maximum achieved from the previous cycle. Finally, peaks in thickness at a_{min} occurred 1.67±0.38 s (mean ± s.e.) after the maximum distance traveled. Posterior progression of the peristaltic wave as well as changes in thickness along the entire length of the worm can be seen over one burrowing cycle (Fig. 5).

Width along the worm also changes over a burrowing cycle, and, from dorsal view images, the peristaltic wave can be seen traveling in the posterior direction as the worm's head backs away from the tip of the crack (Fig. 6). While the worm is moving forward and extending the crack, the anterior part of the body is narrow, and it then widens once the worm reaches the maximum distance traveled for the cycle.

The stress intensity factor (K_I) increases towards the critical stress intensity factor (K_{Ic}) as the distance traveled reaches a local maximum (Fig. 7). The peak in K_I occurs 1.37±0.22 s after the maximum distance for the cycle. The slope of the worm's body at the point of contact with the crack wall, m_a, peaks at nearly the same time as K_I (0.67±0.20 s after the peak in K_I), after distance traveled has reached a local maximum. It then decreases steadily for the rest of the cycle (Fig. 7). The distance from the anterior end of the worm to the point of contact with the crack wall, a, is minimal when K_I reaches a maximum (0.17±0.18 s lag). It then increases linearly and reaches a maximum as distance traveled surpasses the maximum distance achieved on the previous cycle (Fig. 7).

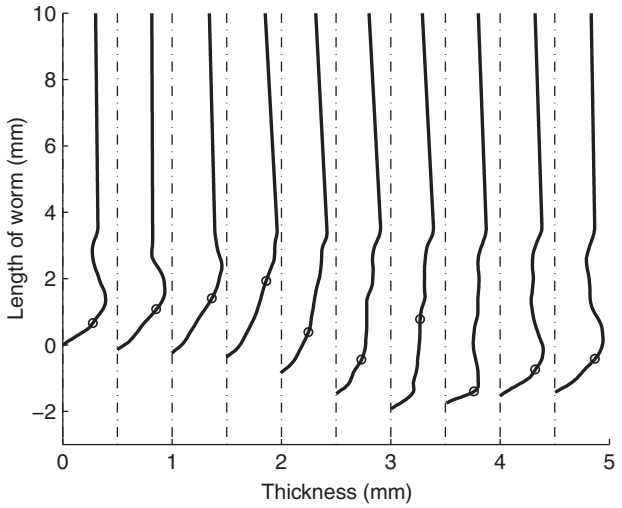

Fig. 5. Waterfall plot of a burrowing cycle for a representative worm (0.02 g wet mass). Half-thickness (solid lines) and midlines (dash-dot lines) of the worm body are shown for frames 1.87 s apart, and the change in thickness with time (on the x-axis). Each outline is offset 0.5 mm from the previous frame. Distance traveled over the burrowing cycle is shown as downward progression of the anterior end of the worm, and a positive forward distance of 1.43 mm is achieved after one cycle. Circles indicate the contact point (a) of the worm with the crack wall.

Dependence of kinematics on body size

Several aspects of worm shape varied with respect to body size for each worm (Table 1). Maximum relative body thickness at a distance 0.05 times the body length from the head tip and at a_{min} decrease as a function of body size (Fig. 8A,B), as predicted by the wedge equation. Relative thickness at the point of contact a also decreases slightly with body size, though not significantly. Relative thickness at h, however, does not depend significantly on body size (Fig. 8C). Also, thickness at each point along the worm's body changes due to the movement of the peristaltic wave. The change in thickness over a burrowing cycle (the amplitude of the peristaltic wave) was measured, and smaller worms exhibited relatively greater changes in thickness than larger worms (Fig. 8D).

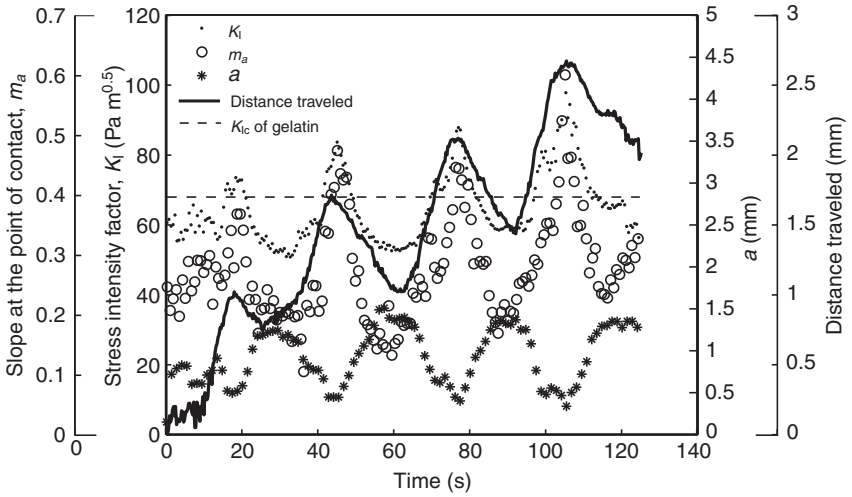

Fig. 7. Stress intensity (K_I, solid circles), slope at the point of contact (m_a, open circles) and distance between the point of contact and anterior of the worm (a, asterisks) plotted over several burrowing cycles, with distance traveled (solid line) and critical stress intensity factor (K_{Ic}, dashed line) as references.

Relative burrowing widths of worms showed no significant trend with body size.

Smaller worms had greater maximum slopes (m_a) at the point of contact a (Fig. 9A), and larger worms had significantly greater maximum stress intensity factors (Fig. 9B). There was no significant trend in minimum a values across worm sizes (Fig. 9C).

The speed of peristaltic waves did not vary among worm sizes. However, smaller worms traveled a greater relative distance per stride than larger worms. Large worms had significantly longer periods for each stride. As a result, overall speed correlates inversely with body size (Fig. 9D).

DISCUSSION

Description of burrowing mechanism

Based on the kinematic data collected, we have described the burrowing cycle as four distinct phases: forward stretching, anterior crack extension, anterior body thickening and peristaltic wave progression (Fig. 3).

In the forward-stretching phase, the worm narrows its anterior end and stretches forwards towards the tip of the crack, but no crack growth occurs. It travels to the point of maximum distance from its previous burrowing cycle. At this point, h is at its maximum, and thickness at a_{min} is at a minimum in comparison to the other phases. Worm width decreases during this phase (Fig. 6). During forward stretching, the worm body appears long, smooth and narrow with no peristaltic wave.

Once at the tip of the crack, the worm enters the anterior crack extension phase. It propagates the crack by becoming slightly thicker and moving forward to the maximum distance for the cycle. During this phase, the anterior of the worm thickens slightly and maintains its thickness during crack extension. The width of the anterior region of the worm is smallest during this phase. K_I increases slightly but remains below K_{Ic}, which was initially puzzling as we expected K_I to reach a maximum as the crack is propagating anteriorly.

The anterior body thickening phase occurs when the worm reaches the maximum distance traveled for the stride. At this point, the anterior region of the body becomes thicker. Maximum thickness of the anterior region, maximum slope at the point of contact a, and minimum a coincide with a peak in K_I as expected since K_I is calculated from a, thickness and slope (see Eqns 5 and 6). There were occasionally discontinuous jumps in K_I as it increased towards the maximum that we attribute to initiation of a new peristaltic wave, causing the point of contact of the worm with the crack wall, a, to move to the anterior dilated region. In some cases, dilatations near the head were formed such that the point of contact moved continuously anteriorly along the worm, but in some cases the dilatation was more abrupt and a new contact point was formed anterior to the previous contact. Although K_I reaches a maximum during this phase, lateral view videos show no sign of anterior crack propagation. This again was surprising as we expected the crack to grow when K_I exceeded K_{Ic}.

The most plausible explanation for why the peak in stress intensity factor occurred after the anterior crack growth phase rather than during crack growth as predicted from fracture mechanics is that the wedge model we used is a 2D model and the width of the worm changes dramatically over the burrowing cycle, potentially violating the assumptions of the model. During crack extension, the anterior region of the worm is much narrower than the rest of the worm

Table 1. Parameters measured from lateral view videos of *Cirriformia moorei*

Parameter	Predicted trend	Actual trend	Statistics
Relative thickness near the anterior end at a_{min}	–	–	R^2=0.19, t=2.087, P=0.051
Relative thickness at 1/20th worm length from the anterior end	–	–	R^2=0.51, t=4.413, P=0.00088
Relative thickness, h	–	0	R^2=0.0060, t=0.327, P=0.75
Relative change in thickness near the anterior end at a_{min}	–	–	R^2=0.42, t=3.740, P=0.0014
Average maximum slope, m_a	–	–	R^2=0.29, t=2.725, P=0.013
Average maximum stress intensity, K_I	+	+	R^2=0.47, t=4.212, P=0.00058
Average minimum value of a	+	0	R^2=0.0090, t=0.426, P=0.66
Average speed	+	–	R^2=0.20, t=2.206, P=0.040

The hypothesized trend for increasing body size and the actual results are shown, as well as the statistics for each correlation. Variables increased (+), decreased (–), or showed no significant correlation (0) with increasing body size.
Degrees of freedom for average maximum slope and average minimum values of a were 18 and for all other parameters were 19.

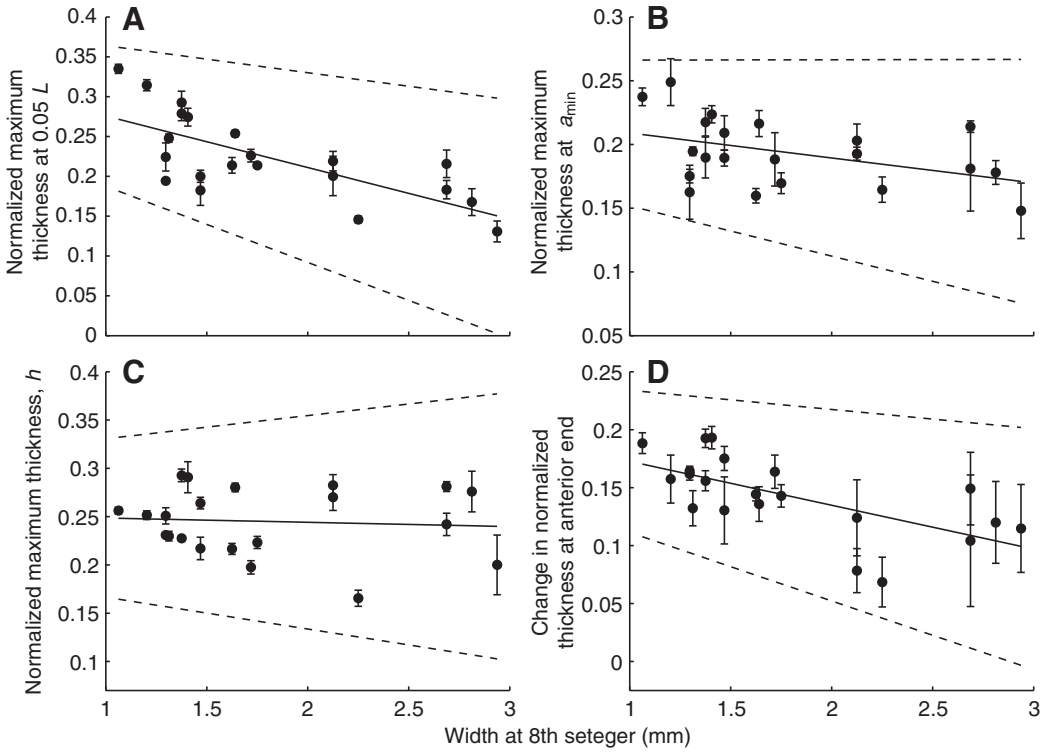

Fig. 8. Normalized thicknesses at 1/20th the worm body length from the anterior end (A), at the anterior end a_{min} (B), normalized thickness h (C), and the variation in normalized thickness over a burrowing cycle (D) plotted as a function of body size. Dependent variables were normalized by dividing by the measured width of the worm at the eighth setiger.

(Fig. 6), which means that the newly formed crack is much narrower than the region of the worm exerting the stress that is amplified at the crack tip. The 2D calculation of stress intensity factor assumes that the width is constant along the entire length of the wedge, so it would underestimate the stress at the narrow crack tip. When the stress intensity factor peaks, the crack may actually be extending laterally even though no anterior crack growth is observed. Both widening (Fig. 6) and thickening (Fig. 4) of the body occur during this phase, initiating a peristaltic wave that may aid in this lateral crack extension. Unfortunately, lateral crack growth was difficult to observe in the dorsal view videos, although it would be consistent with the observed widening of the worm.

Last is the peristaltic wave progression phase, in which peristalsis brings the rest of the body forward into the crack. While the point of maximum body thickness moves in the posterior direction (retrograde peristalsis), the anterior end slips slightly away from the crack tip; a negative change in forward distance is seen (Fig. 3). Overall, distances traveled during the forward-stretching and anterior crack-growth phases outweigh this backward displacement and result in an overall positive distance (forward motion) over the entire cycle.

Comparison with other burrowers

Nereis virens uses its eversible pharynx to generate the stress intensity factor to propagate the crack anteriorly, and it moves its head from side to side to extend the crack laterally (Dorgan et al., 2008). In contrast, to extend the crack anteriorly, *C. moorei* pushes its narrow anterior end forward, using the geometric advantage of exerting a force with a wide body to extend a narrow crack for the head. The use of the hydrostatic skeleton to increase body thickness and achieve a higher stress intensity factor seems to propagate the crack primarily laterally instead of anteriorly. Nevertheless, both the widening of the hydrostatic skeleton and eversion of the pharynx are mechanistically similar in applying a dorsoventral force to propagate the crack. Neither differences in total work to burrow using these different strategies nor resulting permanent deformation of the sediment have yet been explored.

Several other burrowing polychaetes have narrow, pointy heads with few appendages. Glycerids and goniadids have a large eversible proboscis that is used to exert a dorsoventral force on the crack walls similar to *N. virens*, but they can also burrow without proboscis eversion by driving forward their narrow, pointy heads (E. A. K. Murphy and K.M.D., unpublished data). Orbiniids extend a narrow anterior region and use their hydrostatic skeletons rather than eversible probosces or pharynges to exert dorsoventral forces on the crack walls (K.M.D., unpublished data). The mechanical advantage of exerting stress with a wide body to extend a much narrower anterior crack may explain the prevalence of the pointy head.

Effect of size on burrowing kinematics

The wedge equation predicts that for smaller worms, sediments are tougher than for larger worms in similar media. We hypothesized that behaviors would differ between small and large worms consistent with these differing perceptions of the environment. Eqn 3 predicts a higher relative value of h for small worms, but relative body thickness only depends on size near the anterior of the worm. The dominant influence of the anterior region of the body in cracking is consistent, however, with the wedge equations (Eqns 5 and 6) as a greater distance from the anterior of the worm (z) corresponds with a larger value in the denominator and a lower total contribution to K_I. In addition to having a greater relative thickness near the anterior end than larger worms when burrowing, smaller worms had larger relative changes in thickness (amplitude of the peristaltic wave). This increased thickness using the hydrostatic skeleton is consistent with the use of the eversible pharynx by *N. virens* to make the anterior end thicker and blunter when burrowing in tougher materials (Dorgan et al., 2008). We expected smaller worms to be blunter than larger worms to increase their applied stress intensity factor, and they indeed have higher slopes at the point of contact (m_a) when the anterior end thickens. A higher slope at the point of

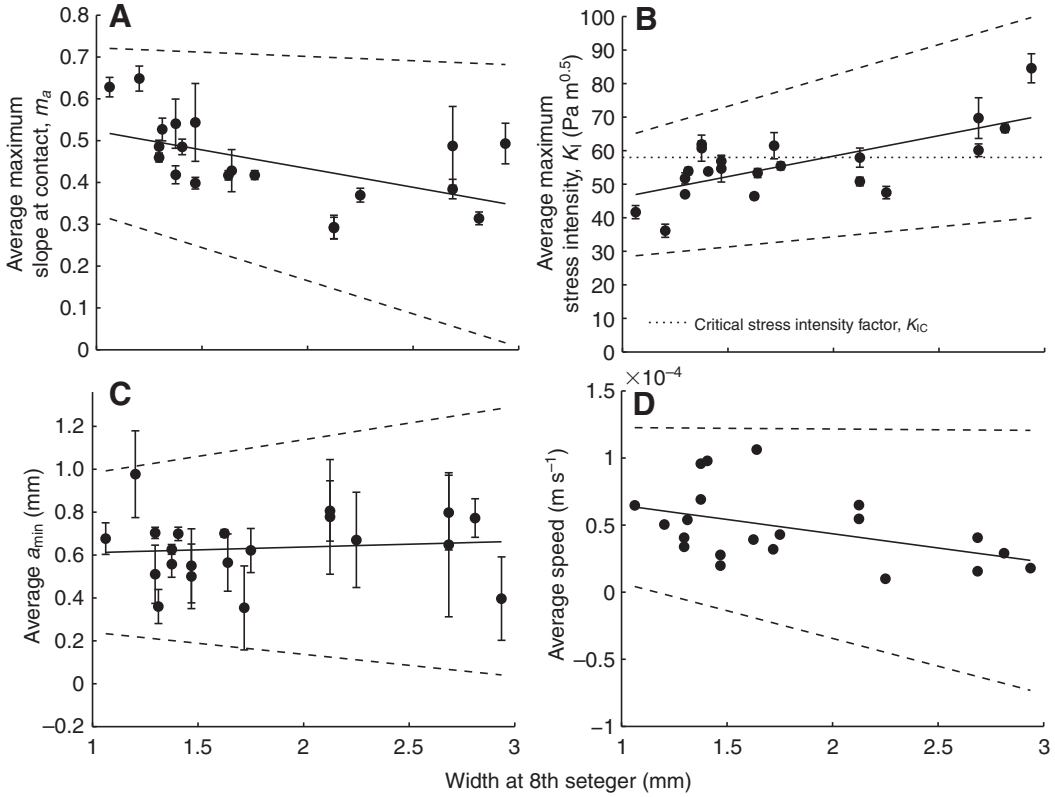

Fig. 9. Average maximum slopes (m_a) at the point of contact a (A), average maximum stress intensity, K_I (B), average a_{min} (C) and average speed of burrowing (D) plotted as a function of body size.

contact enables smaller worms to exert stress closer to the crack tip.

Although smaller worms alter their body shapes to a greater extent than larger worms to increase the stress intensity factor, observations supported the hypothesis that the average maximum K_I increases with body size since larger worms can apply higher stresses with their greater thickness. For large worms (>0.20 g wet mass), peaks in K_I clearly surpassed the critical stress intensity factor, as expected. Some peaks for smaller worms, however, did not exceed K_{Ic}, even though the worms were still able to burrow. This difference likely is an artifact of using a 2D model for a 3D problem, as the stress intensity factor must reach the critical value for the crack to grow as observed. That this discrepancy occurred only for smaller worms is likely just a result of smaller worms exerting smaller K_I, but might also be explained by considering the lateral direction of crack propagation. When burrowing in tougher materials, *N. virens* does not extend the crack edges as far in the lateral direction as it does when burrowing in stiffer materials (Dorgan et al., 2008). Assuming that larger *C. moorei* behave analogously to *N. virens* in a stiffer material, we expect greater lateral crack extension to reduce the elastic force compressing the body of the worm. Because the peak in K_I seems to be associated with lateral crack extension, the increase in K_I with body size could reflect either larger stresses exerted by larger worms or greater lateral crack extension. This is consistent with observations that smaller worms have shorter and fewer gills, and may not need to extend the crack as far laterally to make space for the gills. Unfortunately, dorsal views of body shape relative to the crack edge were not clear enough to show lateral crack growth or the distance between the worm's body and the edge of the crack.

For *C. moorei*, speed of burrowing was negatively correlated with body size, in contrast to the positive correlation between earthworm body size and speed of crawling (Quillin, 1999). For earthworms, the time spent moving increased with body size, whereas the time between forward movements was independent of size (Quillin, 1999). Increases in speed for earthworms were predominantly the result of increased stride length, and stride frequencies were slightly lower in large worms. The inverse relationship between speed and body size for *C. moorei* might be explained by the volume of gills with respect to body size. We observed that larger worms had a noticeably higher volume of gills compared with smaller worms, possibly because larger worms have a smaller surface area to volume ratio and rely more on gills for respiration than smaller worms that may obtain more of their oxygen across the body wall. The long period of the burrowing cycle for large worms might be caused by the time it takes to drag the gills forward along with the anterior end. The need for large worms to cope with the stiffness of the gelatin is another potential issue.

Implications of this study

Here we show that in addition to a dependence on the mechanical properties of sediments (Dorgan et al., 2008), burrowing kinematics depends on body size, consistent with fracture mechanics theory. That body size affects the relative importance of the components of external work done to burrow (fracture and elastic work for small and large worms, respectively) raises interesting questions about animal–sediment interactions in the natural environment. In relatively stiffer sediments, is it energetically advantageous to be smaller? Do either community composition or behaviors of individuals within a community depend on sediment properties, i.e. are stiffer sediments composed of smaller organisms? Do smaller organisms move more than larger organisms in stiffer sediments? Over what spatial and temporal scales do sediment properties vary to a great enough extent to affect burrowing behaviors? Early successional communities tend to be dominated by small organisms living near the sediment–water interface (Pearson and Rosenberg, 1978); how do burrowing and ingestion and egestion of sediments

by early successional communities affect the mechanical properties of sediments? Our results apply only to worms large enough that sediment behaves like a continuum; burrowing mechanics and its dependence on body size for meiofaunal organisms remains an interesting and open question.

Although most long-range particle movement will be related to deposit feeding, the mechanics of burrowing has important implications for small-scale particle mixing. Large deposit feeders in most environments dominate bioturbation because the biodiffusion coefficient scales with the square of the distance that the particle moves (Wheatcroft et al., 1990; Meysman et al., 2008). Particle mixing by small deposit feeders is more appropriately modeled as biodiffusion, in that step distances are smaller and transport is more local (see Choi et al., 2002), although the biodiffusion model does not provide a mechanistic understanding of bioturbation (see Meysman et al., 2003). In addition, smaller deposit feeders are often abundant and active, decreasing the time between particle movements. We have shown that burrowing behavior depends on body size, but whether and how these differences translate to particle mixing are unknown. The greater relative amplitude of the peristaltic wave for small burrowers may result in increased particle mixing, although large worms still exert larger absolute forces, potentially resulting in greater permanent deformation. In addition, the interdependence of fracture toughness, stiffness and body size in affecting burrowing behavior suggests that the effects of burrower size on particle mixing depend on the mechanical properties of the sediment. Additional complexity arises from the poorly understood dependence of the response of sediments to forces on their mechanical properties. Clearly, more research is needed on the mechanical responses of sediments to varying forces exerted over different areas and times as well as fracture dynamics in different sediments (i.e. how easily particles or aggregates are fractured from the bulk sediment) to link burrowing behavior to particle mixing.

We find it particularly intriguing that although the mechanics are similar, *Cirriformia* shows substantial differences in shape and behavior from *Nereis* and wonder how many other styles or modes of burrowing may be found among the polychaetes and other vermiform taxa.

LIST OF SYMBOLS AND ABBREVIATIONS

a	distance from the tip of the crack to the point of contact between the anterior end of the worm and the crack wall
a_c	half-width of a bubble in a medium
a_{max}	average maximum value of a achieved for each cycle
a_{min}	average minimum value of a achieved for each cycle
b	distance between the anterior end of the worm and the tip of the crack
E	modulus of elasticity (Pa)
G_c	crack resistance, critical energy release rate ($J\,m^{-2}$)
h	half-thickness of a worm at a point far away from the anterior end
K_I	stress intensity ($Pa\,m^{0.5}$)
K_{Ic}	critical stress intensity factor ($Pa\,m^{0.5}$)
m_a	slope of the worm body at its point of contact a
p_r	point on a regression line through the midpoints of a worm contour
w_{crack}	width of a crack in a medium (m)
W_{cr}	work to extend crack by fracture
w_{worm}	width of a worm body in a medium (m)
W_{El}	work to deform elastic material
Wg	'wedge' number (dimensionless)
z	the distance from the anterior of the worm
δ_c	the half-thickness of a bubble
Δx	distance of crack growth
ν	Poisson's ratio (dimensionless)

ACKNOWLEDGEMENTS

We thank M. A. R. Koehl, P. A. Jumars, F. Meysman and an anonymous reviewer for helpful comments on the manuscript. This project was funded by NSF IOS grant #0642249 to M. A. R. Koehl, as well as from the Virginia G. and Robert E. Gill Chair to M. A. R. Koehl and the Undergraduate Research Apprenticeship Program, University of California, Berkeley.

REFERENCES

Anderson, T. L. (1995). *Fracture Mechanics: Fundamentals and Applications*. Boca Raton, FL: CRC Press.

Barenblatt, G. I. (1962). The mathematical theory of equilibrium cracks in brittle fracture. In *Advances in Applied Mechanics*, vol. 7 (ed. H. L. Dryden and T. von Karman), pp. 55-129. New York, NY: Academic Press.

Blake, J. A. (1996). Family Cirratulidae. In *Taxonomic Atlas of the Santa Maria Basin and Western Santa Barbara Channel*, Vol. 6, *Annelida*, Part 3, *Polychaeta: Orbiniidae to Cossuridae* (ed. J. A. Blake, B. Hilbig and P. H. Scott), pp. 263-384. California: Santa Barbara Museum of Natural History.

Boudreau, B. P., Algar, C., Johnson, B. D., Croudace, I., Reed, A., Furukawa, Y., Dorgan, K. M., Jumars, P. A., Grader, A. S. and Gardiner, B. S. (2005). Bubble growth and rise in soft sediments. *Geology* **33**, 517-520.

Choi, J., Francois-Carcaillet, F. and Boudreau, B. P. (2002). Lattice-automaton bioturbation simulator (LABS): implementation for small deposit feeders. *Comput. Geosci.* **28**, 213-222.

Dorgan, K. M., Jumars, P. A., Johnson, B. D., Boudreau, B. P. and Landis, E. (2005). Burrow elongation by crack propagation. *Nature* **433**, 475.

Dorgan, K. M., Jumars, P. A., Johnson, B. D. and Boudreau, B. P. (2006). Macrofaunal burrowing: the medium is the message. *Oceanogr. Mar. Biol.* **44**, 85-141.

Dorgan, K. M., Arwade, S. R. and Jumars, P. A. (2007). Burrowing in marine muds by crack propagation: kinematics and forces. *J. Exp. Biol.* **210**, 4198-4212.

Dorgan, K. M., Arwade, S. R. and Jumars, P. A. (2008). Worms as wedges: Effects of sediment mechanics on burrowing behavior. *J. Mar. Res.* **66**, 219-254.

Hentschel, B. T. (1998). Intraspecific variations in $\delta^{13}C$ indicate ontogenetic diet changes in deposit-feeding polychaetes. *Ecology* **79**, 1357-1370.

Johnson, B. D., Boudreau, B. P., Gardiner, B. S. and Maass, R. (2002). Mechanical response of sediments to bubble growth. *Mar. Geol.* **187**, 347-363.

Jumars, P. A. and Gallagher, E. D. (1982). Deep-sea community structure: three plays on the benthic proscenium. In *The Environment Of The Deep Sea* (ed. W. G. Ernst and J. G. Morin), pp. 217-255. Englewood Cliffs, NJ: Prentice-Hall.

Mahon, H. K. and Dauer, D. M. (2005). Organic coatings and ontogenetic particle selection in *Streblospio benedicti* Webster (Spionidae: Polychaeta). *J. Exp. Mar. Biol. Ecol.* **323**, 84-92.

Mayer, L. M., Jumars, P. A., Taghon, G. L., Macko, S. A. and Trumbore, S. (1993). Low-density particles as potential nitrogenous foods for benthos. *J. Mar. Res.* **51**, 373-389.

Meysman, F. J. R., Boudreau, B. P. and Middelburg, J. J. (2003). Relations between local, nonlocal, discrete and continuous models of bioturbation. *J. Mar. Res.* **61**, 391-410.

Meysman, F. J. R., Middelburg, J. J. and Heip, C. H. R. (2006). Bioturbation: a fresh look at Darwin's last idea. *Trends Ecol. Evol.* **21**, 688-695.

Meysman, F. J. R., Malyuga, V. S., Boudreau, B. P. and Middelburg, J. J. (2008). A generalized stochastic approach to particle dispersal in soils and sediments. *Geochim. Cosmochim. Acta* **72**, 3460-3478.

Pearson, T. H. and Rosenberg, R. (1978). Macrobenthic succession in relation to organic enrichment and pollution of the marine environment. *Oceanogr. Mar. Biol. Annu. Rev.* **16**, 229-311.

Penry, D. L. and Jumars, P. A. (1990). Gut architecture, digestive constraints and feeding ecology of deposit-feeding and carnivorous polychaetes. *Oecologia* **82**, 1-11.

Quillin, K. J. (1998). Ontogenetic scaling of hydrostatic skeletons: geometric, static stress and dynamic stress scaling of the earthworm *Lumbricus terrestris*. *J. Exp Biol.* **201**, 1871-1883.

Quillin, K. J. (1999). Ontogenetic scaling of peristaltic crawling in the earthworm *Lumbricus terrestris*. *J. Exp. Biol.* **202**, 661-674.

Quillin, K. J. (2000). Ontogenetic scaling of burrowing forces in the earthworm *Lumbricus terrestris*. *J. Exp. Biol.* **203**, 2757-2770.

Rossi, F., Herman, P. M. J. and Middelburg, J. J. (2004). Interspecific and intraspecific variation of $\delta^{13}C$ and $\delta^{15}N$ in deposit- and suspension-feeding bivalves (*Macoma balthica* and *Cerastoderma edule*): evidence of ontogenetic changes in feeding mode of *Macoma balthica*. *Limnol. Oceanogr.* **49**, 408-414.

Shull, D. H. and Yasuda, M. (2001). Size-selective downward particle transport by cirratulid polychaetes. *J. Mar. Res.* **59**, 453-473.

Sih, G. C. (1973). *Handbook Of Stress Intensity Factors: Stress Intensity Factor Solutions And Formulas For Reference*. Bethlehem, PA: Lehigh University.

Timoshenko, S. P. and Goodier, J. N. (1970). *Theory Of Elasticity*, 608 pp. New York: McGraw-Hill.

Wheatcroft, R. A., Jumars, P. A., Smith, C. R. and Nowell, A. R. M. (1990). A mechanistic view of the particulate biodiffusion coefficient: step lengths, rest periods and transport directions. *J. Mar. Res.* **48**, 177-207.